Pergamon

PII: S0045-7930(96)00016-3

Computers & Fluids Vol. 26, No. 4, pp. 395–415, 1997

Printed in Great Britain
0045-7930/97 $17.00 + 0.00

A NUMERICAL MODEL OF SLUG FLOW IN VERTICAL TUBES

A. CLARKE and R. I. ISSA*

Department of Mechanical Engineering, Imperial College of Science, Technology & Medicine, Exhibition Road, London SW7 2BX, U.K.

(Received 22 May 1995; in revised form 23 April 1996)

Abstract—This paper presents a numerical method for the determination of the flow field structure in slug flow in vertical tubes. The method is based on the ensemble averaged transport equations governing the flow of the liquid around the Taylor bubble and in the slug, which together comprise one slug unit. Turbulence is accounted for by the k–ϵ model. An iterative scheme is used to compute the shape and velocity of the Taylor bubble simultaneously with the flow field; the conditions which are taken to determine these quantities are uniform bubble pressure and smoothness of the bubble nose. The equations are discretised using a finite volume technique on a block structured, non-orthogonal mesh which conforms to the flow domain boundary. The predicted velocities of a single Taylor bubble rising in both stagnant and moving liquid agree very well with experimental data. For a train of Taylor bubbles in periodic slug flow, the computed bubble rise velocity and pressure gradient agree well with the data provided that account is taken of the presence of dispersed gas in the liquid slug. © 1997 Elsevier Science Ltd.

NOMENCLATURE

$a_\bullet$ = coefficient of momentum equation associated with node ●
A = area of cell face
C_{01} = Froude number in stagnant liquid
C_{02} = empirical coefficient
C_1, C_2, C_μ = turbulence model constants: $C_1 = 1.44$; $C_2 = 1.92$; $C_\mu = 0.09$
d = coefficient of the pressure gradient in the momentum equations
D = tube diameter
E = elastic modulus
$f_i^{ic}(n)$ = force acting on interconnection ic to node n in direction i
F_e = mass flux at cell face e
g = gravitational constant
G = generation of turbulent kinetic energy
ic = interconnection between two nodes
k = turbulent kinetic energy
l = length scale
L_{ic} = length of interconnection ic
p = static pressure
p^* = piezometric pressure
p_0 = stagnation pressure at nose of Taylor bubble
Pr_k = Prandtl number of k
Pr_ϵ = Prandtl number of ϵ
Re_L = liquid Reynolds number
S_k = source term for k
S_ϵ = source term for ϵ
u_{in} = relative velocity in ith coordinate direction
v = relative velocity aligned with bubble surface
U_c = centreline liquid velocity
U_{in} = absolute inlet velocity in ith coordinate direction
U_{SL} = superficial liquid velocity
U_{SG} = superficial gas velocity
U_{STB} = Taylor bubble velocity in stagnant liquid
U_{TB} = absolute velocity of Taylor bubble
u_{wall} = relative velocity of wall
Xn_{ij} = coordinate of jth node in direction i
θ_j^c = isoparametric function at jth corner node
θ_j^m = isoparametric function at jth midedge node

* Corresponding author.

α = dispersed gas void fraction
δv = cell face velocity increments
δp = pressure discrepancies
σ_{ij} = stress tensor
ϵ = dissipation of turbulent kinetic energy
μ = mixture viscosity
μ_{eff} = effective viscosity
μ_g = gas viscosity
μ_l = liquid viscosity
μ_t = turbulent viscosity
ρ = mixture density
ρ_g = gas density
ρ_l = liquid density
τ_w = wall shear stress
ϕ $(= \tau_w/\rho g h)$ = saturation

1. INTRODUCTION

One of the most frequently encountered regimes in two phase flow in pipes is slug flow and it occurs in the chemical process, nuclear and petroleum industries. Prediction of the usual important parameters, namely pressure drop along the pipe and the gas content in the slug, which are of interest to the engineer, has in the past been obtained from empirical correlations derived from laboratory data that do not always extrapolate to conditions existing in practical applications (see, for example, Fancher and Brown [1], Hughmark [2], Yocum [3], Duns and Ross [4] and Griffith and Wallis [5]). Such correlations are therefore neither general nor reliable. In order to provide better predictions, semi-mechanistic approaches have also been resorted to whereby a flow analysis is made using one slug unit consisting of one Taylor bubble and the liquid slug behind it; examples of such analyses are those of Fernandes *et al.* [6], Orell and Rembrand [7] and Issa and Tang [8]. In this type of analysis, overall balance equations are formulated for mass and momentum within the different sections of the slug unit. Alas, much empiricism creeps back into such analyses thereby undermining the fundamental basis of the approach. Fernandes *et al.* [6] devised such a model by taking mass balances over the entire slug unit as well as the falling film to derive relationships for flow variables such as the velocity of the gas in the Taylor bubble, the velocity of the liquid slug and the average voids. Empirical correlations are used to obtain other quantities such as the velocity of the Taylor bubble and of the bubbles within the liquid slug. This led to a system of 17 non-linear coupled equations which when solved showed good agreement of bubble/slug length ratios and average void fractions over the slug unit with experiments conducted by the same authors. Orell and Rembrand [7] proposed a simpler model comprising only seven non-linear equations. Their model differed from that of Fernandes *et al.* in that they considered a force balance for the flow around the Taylor bubble nose to derive a relationship between the film velocity, the Taylor bubble velocity and the gas void fraction, whereas the Fernandes *et al.* model employs correlations for this purpose. More recently, Issa and Tang [8] developed a model on similar lines to that of Fernandes *et al.* but incorporating some of the features of the Orell and Rembrand model, namely the velocity profile in the falling film. The resulting system consisted of only six equations which when solved gave fairly good results for the average void fractions.

One of the main inputs required in the above semi-empirical analyses is the rise velocity of the Taylor bubble, and this has received considerable attention in the past. Theoretical approaches have been concerned with single bubble dynamics, and more specifically the inviscid flow around the nose of a Taylor bubble whose base is assumed to exert no influence on the rise velocity. Such an approach has been successfully applied using potential flow theory by Dumitrescu [9], and Davies and Taylor [10], who derived an expression for the rise velocity of a single Taylor bubble in stagnant liquid

$$U_{\text{STB}} = C_{01}\sqrt{gD} \tag{1}$$

where U_{STB} is the rise velocity of the Taylor bubble in stagnant liquid. The coefficient C_{01} is a Froude number which takes the value of 0.35 according to Dumitrescu [9] or 0.33 according to Davies and Taylor [10], the difference in these values being due to the degree of approximation used. Nonetheless, both are in close agreement with the experimental value of 0.345 (see, for example, Harmathy [11] and Nicklin *et al.* [12]). This approach was advanced by Collins [13, 14], Nickens and Yannitell [15] and many others. The extension of the potential flow theory to account for

moving liquid requires the viscous effects to be incorporated into the solution by prescribing the vorticity from an assumed velocity profile upstream of the Taylor bubble, while assuming an inviscid flow around the bubble nose. Collins *et al.* [14] have employed such an approach for the case of a single Taylor bubble rising in both laminar and turbulent flowing liquid to find an analytical solution of the form

$$U_{TB} = U_c + (gD)^{\frac{1}{2}}\phi\left(\frac{U_c}{\sqrt{gD}}\right) \tag{2}$$

where U_c is the centreline liquid velocity and ϕ is some function of the centreline Froude number. Their results for turbulent flow showed good agreement with the experimental results of Nicklin *et al.* [12], although their laminar flow results were found to be inaccurate. Bendiksen [16] suggested that the discrepancy in the laminar results was due to the neglect of surface tension and inclusion of this in his model produced much better agreement with his own experiments and with those of Nicklin *et al.* Equation (2) gives support to the suggested empirical correlation of Nicklin *et al.*

$$U_{TB} = U_{STB} + C_{02}U_{SL} \tag{3}$$

where U_{SL} is the superficial liquid phase velocity and C_{02} is an empirical coefficient found to be 1.2 for $Re_L > 8000$ and to vary up to 1.8 as Re_L decreases to zero. Bendiksen has also experimentally confirmed the value of C_{02} to be 1.2 for Re_L in the range 5000–110,000 for a single bubble rising in a gas free liquid, and Frechou [17], Fernandes [18] and Mao and Duckler [19] have all found this value to also apply to slug flow in which the liquid slug contains gas bubbles in dispersed form; in such flow, however, U_{SL} in equation (3) must be replaced by the superficial mixture velocity.

Potential flow theory is limited and does not yield much more information than the rise velocity of the bubble. An alternative more general and flexible approach is a fully mechanistic one which calculates the entire flow around and behind the Taylor bubble and which simultaneously determines both the shape and rise velocity of the Taylor bubble. Mao and Duckler [20, 21] have developed a method for determining the shape and rise velocity of a single axisymmetric Taylor bubble rising in stagnant or flowing liquid. The two-dimensional Navier–Stokes equations were solved for gas-free liquid flowing ahead and around the bubble up to its base using a finite volume method in conjunction with a cylindrical polar mesh. However, the flow behind the base of the bubble was excluded from the calculation. Turbulence was incorporated into the model by means of the low Reynolds number k–ϵ model of Nagano and Hishida [22], where a damping factor was employed to adjust the turbulent viscosity at the wall and in the liquid film between the wall and the Taylor bubble interface. For the bubble shape determination a first-order differential equation was derived from approximate momentum considerations which when solved gave the area change at each cross-section of the Taylor bubble to satisfy a constant bubble pressure condition. The rise velocity was determined by trial and error, with the final correct velocity producing a bubble nose which was locally spherical at the stagnation point. The rise velocity and shape were found by Mao and Duckler [19] to be in very good agreement with their own experiments and with the data of Collins *et al.* [14].

The purpose of the present investigation is to develop a new mechanistic model that is more general and accurate than that of Mao and Duckler and is not restricted to single Taylor bubbles but can also deal with periodic slug flow. This is achieved by including into the analysis the flow field behind the base of the bubble as well as around its nose. Such an analysis is enabled by the use of a finite volume numerical solution procedure based on non-orthogonal block structured meshes which can map the entire flow field around the Taylor bubble and in the liquid slug behind it. The motion of the gas in the Taylor bubble is ignored and the liquid may be either laminar or turbulent and turbulence is accounted for by the use of the k–ϵ model. The use of the non-orthogonal mesh enables the precise alignment of the mesh with the interface between the bubble and the liquid, a feature which could not be effected in the polar mesh of Mao and Duckler. A new method is developed here for locating the interface whereby a general relation based on local conditions is used to displace the interface in search of a constant bubble pressure. The bubble rise velocity was determined using the same practice developed in the cited reference; however, in the present work, the flow around the base of the bubble is also considered although the base itself is assumed to be flat. The assumption that the base of the bubble is flat requires justification. At

low velocities, experimental evidence shows that the base of the Taylor bubble is indeed almost flat; computations performed with this assumption for these conditions showed that the pressure variations across the base are negligible, thereby confirming that the assumption is valid for such cases. However, at higher velocities the base is known to become concave with 'pinched' edges. In fact, under these conditions it is difficult to identify a base at all since the flow is highly agitated with a multitude of small bubbles being shed from the rear of the Taylor bubble. Such a phenomenon needs to be modelled separately and is beyond the scope of the present work. Some of the results presented herein are therefore subject to the above approximation. It is interesting to point out here that attempts at applying the surface adjustment algorithm presented herein to the bubble base quickly resulted in an unstable surface, and the computations could not be continued since they were performed under the assumption of steady-state flow. This suggests that the base instability which is observed in real slug flow is being captured to some extent by the present method. A full simulation of the phenomenon would however require appropriate extension to transient flow.

For single bubble dynamics, the inlet boundary conditions for both of the above approaches can easily be obtained from an analysis of the liquid in the pipe ahead of the bubble. However, to perform the same analysis for the case of slug flow, where the train of Taylor bubbles are separated by slugs of liquid and rise consecutively, the boundary conditions at the inlet cross-section of the slug unit are not known in advance and must be determined as an outcome of the solution. This is achieved by the imposition of cyclic conditions at the inlet and outlet of the slug unit whose bubble/slug length ratio is known. This is based on the assumption that the flow pattern repeats itself over consecutive slug units. The presence of dispersed gas in the liquid slug is accounted for approximately by assuming homogeneous flow within the liquid slug. The method solves the inverse problem in that it computes the bubble velocity for a given liquid flow rate and bubble/slug length ratio. This determines the gas flow rate and the pressure drop which is deduced from the computed flow field. Usually, it is the flow rates of the two phases that are given and the bubble/slug length ratio which is unknown. In such cases, the method can still be used in a guess and correct fashion whereby the bubble/slug length ratio is continually adjusted to give the required gas flow rate.

2. GOVERNING EQUATIONS

Slug flow features the transport of a train of Taylor bubbles separated by liquid slugs containing smaller dispersed bubbles. For the present investigation, the case of fully developed slug flow will be considered in which Taylor bubbles and liquid slugs rise without acceleration, and hence the lengths of both Taylor bubble and liquid slugs remain constant. This makes the analysis of the flow field tractable by allowing a steady-state calculation to be performed for one slug unit comprising one Taylor bubble and the liquid slug separating two successive bubbles. It is assumed that the circulatory flow of the gas within the Taylor bubble is of little consequence on the outer liquid flow field. This is reasonable as the density and viscosity ratios are usually very high leading to conditions closely approximating full slip at the interface between liquid and gas. The most important condition of which knowledge is required here is how the pressure varies within the Taylor bubble. This is taken to be uniform in correspondence with experimental evidence.

A steady-state analysis is enabled by a coordinate transformation in which the frame of reference is attached to the Taylor bubble travelling at an absolute velocity of U_{TB}. With the new coordinates (see Fig. 1), the bubble now becomes stationary and the pipe wall moves with a velocity u_{wall} given by

$$u_{wall} = -U_{TB}\,. \tag{4}$$

The transport equations governing the liquid flow are those of mass continuity and momentum which in Cartesian tensor notations are, respectively

$$\frac{\partial}{\partial x_i}(\rho u_i) = 0 \tag{5}$$

$$\frac{\partial}{\partial x_j}(\rho u_j u_i) = -\frac{\partial p^*}{\partial x_i} + \frac{\partial \sigma_{ij}}{\partial x_j} \tag{6}$$

where u is the relative velocity and p^* is the piezometric pressure defined by

$$p^* = p + \rho g z \tag{7}$$

and z is the vertical distance measured upwards from a datum.

In continuous slug flow, it is well known that small bubbles are shed continuously from the base of each Taylor bubble, into the liquid slug behind it. At the same time, a corresponding quantity of small dispersed bubbles is entrained at the nose of the Taylor bubble, thus balancing the rate of loss of gas from it due to shedding. Unlike previous numerical models, the present model attempts to account for the presence of these small dispersed bubbles in the liquid slug, albeit in a simplistic manner. Here, the liquid phase is taken to contain gas bubbles in dispersed form which is assumed not to alter the flow field in the slug section except through modification of the viscosity and density of the liquid/gas slug mixture. This corresponds to the assumption of homogeneous two phase flow which is not a strictly valid approximation since it is known that such small bubbles are unevenly distributed within the liquid slug. However, it is supposed in the present work that the relative motion between these bubbles and the liquid and the non-uniform distribution of the phase fraction in the liquid slug may be ignored as a first-order approximation.

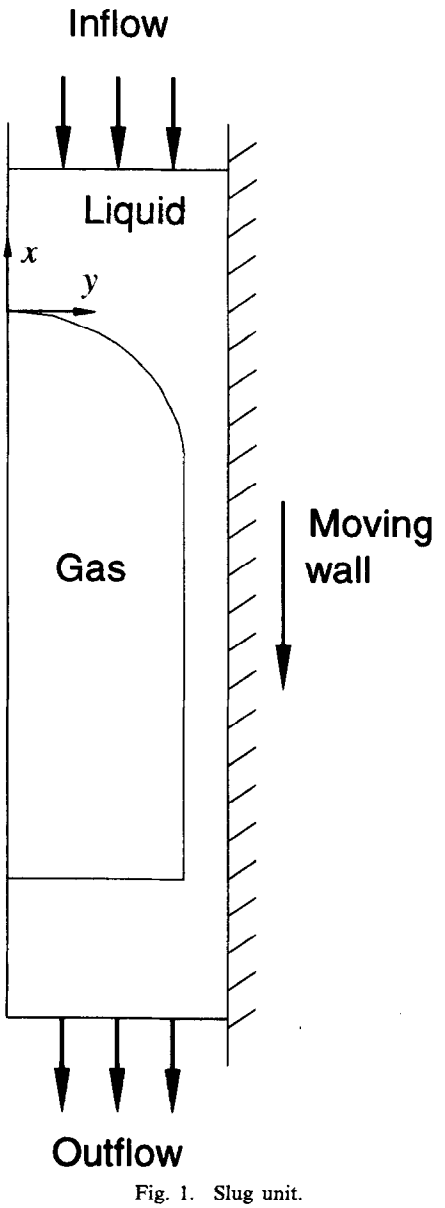

Fig. 1. Slug unit.

Thus

$$\rho = \rho_l(1 - \alpha) + \rho_g\alpha \tag{8}$$

$$\mu = \mu_l(1 - \alpha) + \mu_g\alpha \tag{9}$$

where α is the mean gas void fraction in the slug. For the case of single bubble motion the value of α is taken as zero which corresponds to gas-free liquid. This assumption does not apply in the case of periodic slug flow where there are many small bubbles of gas dispersed in the liquid slug, and they may not be ignored. In this case the value of α is estimated to be between 20 and 30% as shown by experimental evidence [6]. For the present, the specification of α and the use of equations (8) and (9) are the main empirical information introduced into the model. In the future, such approximation has to be eliminated and the model needs to be extended to compute the void fraction field, possibly by solving for the two fluids (gas and liquid) within the slug; this, however, would require a major extension of the model and will require modelling of the gas entrainment by and shedding from the Taylor bubble.

Now the relative velocity of the liquid at any point in the streamwise direction is defined as

$$u_{in} = U_{in} - U_{TB} \tag{10}$$

where U_{in} is defined as the absolute inlet velocity. Turbulence effects are incorporated into the model by means of the standard high Reynolds number k–ϵ model in which the stress tensor σ_{ij} is related to the rate of strain field for a Newtonian fluid by

$$\sigma_{ij} = \mu_{eff}\left[\left(\frac{\partial u_i}{\partial x_j} + \frac{\partial u_j}{\partial x_i}\right) - \frac{2}{3}\delta_{ij}\left(\frac{\partial u_k}{\partial x_k} + k\right)\right] \tag{11}$$

where

$$\mu_{eff} = \mu + \mu_t \tag{12}$$

$$= \mu + \frac{C_\mu \rho k^2}{\epsilon} \tag{13}$$

is the effective viscosity composed of a laminar part μ and a turbulent part μ_t. k is the turbulent kinetic energy and ϵ is its rate of dissipation, each of which obeys its own transport equation

$$\frac{\partial}{\partial t}(\rho k) + \frac{\partial}{\partial x_j}(\rho u_j k) = \frac{\partial}{\partial x_j}\left(\frac{\mu_t}{Pr_k}\frac{\partial k}{\partial x_j}\right) + S_k \tag{14}$$

$$\frac{\partial}{\partial t}(\rho \epsilon) + \frac{\partial}{\partial x_j}(\rho u_j \epsilon) = \frac{\partial}{\partial x_j}\left(\frac{\mu_t}{Pr_\epsilon}\frac{\partial \epsilon}{\partial x_j}\right) + S_\epsilon \tag{15}$$

where

$$S_k = G - \rho\epsilon \tag{16}$$

$$S_\epsilon = \frac{C_1 \epsilon G}{k} - \frac{C_2 \rho \epsilon^2}{k} \tag{17}$$

$$G = \mu_t \frac{\partial u_i}{\partial x_j}\left(\frac{\partial u_i}{\partial x_j} + \frac{\partial u_j}{\partial x_i}\right) \tag{18}$$

and $Pr_\epsilon = 1.3$, $Pr_k = 1.0$, $C_\mu = 0.09$, $C_1 = 1.43$ and $C_2 = 1.92$.

The above k–ϵ model is appropriate for high Re flows and is invalid for low Re flows. In the present work, attention was paid to ensure that all cases computed fell in the former category for which the turbulence model is valid.

The equations are solved subject to the following boundary conditions. At the pipe axis, symmetry corresponding to axisymmetric conditions in vertical slug flow is imposed. No-slip boundary conditions are applied at the pipe wall, i.e. $u = u_{wall}$. Wall functions are employed to

account for the steep variations in the fluid properties caused by the turbulent motion, details of which may be found in Launder and Spalding [23]. On the Taylor bubble interface, a full-slip condition is used whereby the gradients normal to the interface of the velocity component tangential to the surface vanish; also the relative velocity component normal to the surface is put to zero. The no-slip condition on the interface between gas and liquid is tantamount to the condition of zero shear stress. This is a reasonable assumption in view of the low viscosity ratio: the shear stress exerted at the interface by the gas is negligible compared to those generated in the rest of the liquid flow field. For a single Taylor bubble, the inflow conditions are prescribed far upstream of the bubble, while the outflow conditions are extrapolated from the interior. To simulate fully developed slug flow, periodic conditions are imposed at the inflow and outflow boundaries of the representative slug unit; velocities at these boundaries are forced to return to the prescribed flow rate. Initially, the inflow velocity profile is specified to satisfy the given mass flow rate, and the level of turbulence is taken as a percentage of the mean kinetic energy, while its dissipation is calculated according to

$$\epsilon = \frac{C_\mu k^{1.5}}{l} \tag{19}$$

where l is an appropriate length scale. The computed dependent variable profiles at the outlet are then imposed (after adjustment to give the desired mass flow rate) at the inflow boundary after each iteration until convergence is attained when the solution obeys the cyclically repeating conditions at inflow and outflow. The level of turbulence is thus determined purely from the effects of the wall and the flow around the Taylor bubble. The pressure is linearly extrapolated from the interior to all boundaries. However, the pressure at the interface must be uniform and this corresponds to the unique shape of the Taylor bubble; it is this condition that is invoked to determine the bubble shape.

3. DISCRETISATION AND METHOD OF SOLUTION

The above equations are solved numerically by use of a finite volume method which utilises a non-orthogonal boundary-fitted mesh with all variables stored at cell centres (see Fig. 2 where a portion of the mesh is depicted). The velocity components solved for are those aligned in the axial and radial directions, respectively. The mass fluxes at cell faces are calculated from the cell-centred velocities by the pressure-weighted interpolation of Rhie and Chow [24] which couples the velocity and pressure fields together. The finite difference approximations used to represent the convective and diffusive fluxes are the standard upwind and centred schemes, respectively. Details of the discretisation can be found elsewhere (e.g. Peric [25]) and are hence omitted here.

The non-orthogonal mesh used is block structured and is generated as follows: the domain is first divided into hexahedral subdomains. Each subdomain is transformed onto a unit cube in transformed space (ξ,η,ζ) where it is meshed. It is then transformed back to the physical space (x,y,z) by the transformation

$$x_i = \sum_j \theta_j(\xi,\eta,\zeta) XN_{ij} \tag{20}$$

where XN_{ij} are the coordinates of the j nodes specifying a subdomain and Θ_j are the isoparametric functions [26] given by

$$\theta_j^{\mathrm{c}}(\xi,\eta,\zeta) = \frac{1}{8}(1 + \xi_j\xi)(1 + \eta_j\eta)(1 + \zeta_j\zeta)(\xi_j\xi + \eta_j\eta + \zeta_j\zeta - 2) \tag{21}$$

$$\theta_j^{\mathrm{m}}(\xi,\eta,\zeta) = \frac{1}{4}(1 - \xi^2)(1 + \eta_j\eta)(1 + \zeta_j\zeta) \tag{22}$$

where the superscripts c and m refer to corner and midedge nodes, respectively.

The set of algebraic equations resulting from the discretisation process is solved by the pressure-correction algorithm SIMPLE [27]. The overall algorithm which is an iterative one is adapted here to determine two other unknowns: the shape of the Taylor bubble and the velocity of the Taylor bubble U_{TB}. The adaptation is described next.

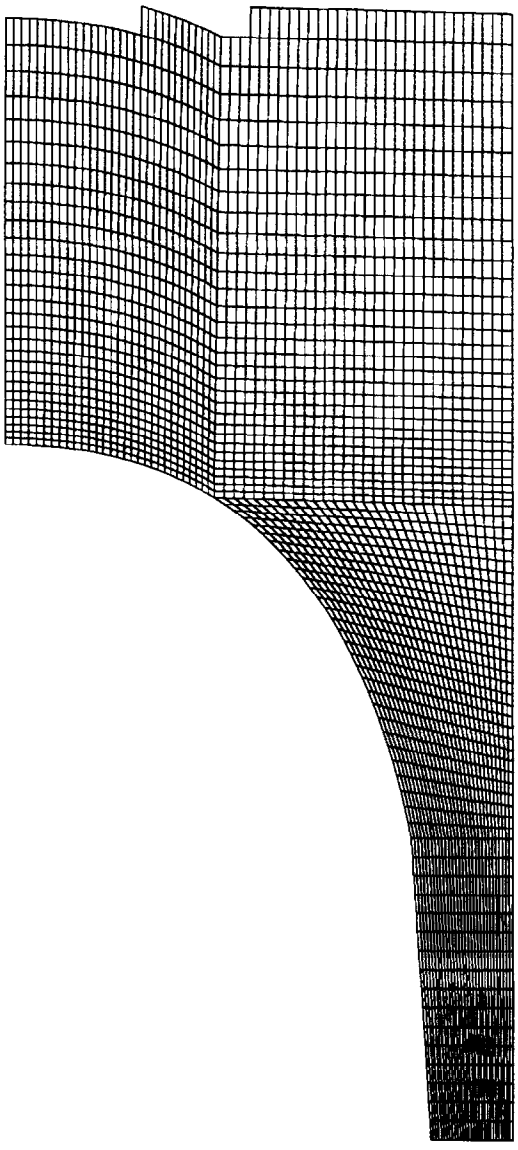

Fig. 2. Non-orthogonal boundary fitted mesh in the vicinity of the Taylor nose bubble.

For a guessed Taylor bubble shape, the solution of the liquid flow field will result in a pressure (on the gas side) at the interface which is not uniform unless the correct bubble shape is assumed. To eliminate this non-uniformity, the interface has to be displaced at every point (the distance of displacement being calculated locally from the pressure discrepancy) via a relationship given in the next section. This process is repeated either at every outer iteration of the solution algorithm or after every few iterations, until convergence to the correct shape that yields a uniform interface pressure is achieved.

The base of the bubble is exempted from the above treatment, and is assumed to be flat. This assumption was made in order to accelerate and stabilize the iteration process and was indeed found to be sufficiently accurate for some of the cases computed. The other quantity that has to be determined iteratively is the bubble velocity. This was achieved in the same manner as was done by Mao and Duckler [21]: an incorrectly guessed value of U_{TB} will yield a bubble nose which is not locally spherical at the stagnation point; only one unique value of U_{TB} gives this tangency condition at the nose and it is this value which is taken to be the correct one. The value of U_{TB} ($= u_{wall}$) is therefore adjusted continuously within the iteration process to arrive at the correct rise velocity.

The steps involved in the overall solution procedure are as follows:

1. From the latest guess of the Taylor bubble shape, a boundary fitted mesh, with one mesh surface aligned with the interface, is generated.
2. The discretised momentum equations with the latest pressure field are solved to obtain the velocity field; the wall velocity used for the boundary condition is the latest guess of U_{TB}.
3. The pressure correction equation is solved to obtain an updated pressure field; the velocities are also adjusted so as to satisfy continuity.
4. The scalar equations for the turbulent quantities k and ϵ are solved to find the turbulent viscosity.
5. The profiles of the computed field variables at the outflow plane are now imposed at inflow to accord with the cyclic boundary condition treatment. This step is omitted for the case of single bubble motion.
6. The interface pressure is determined by linear extrapolation from the interior pressure field (taking into account surface tension effects). This will not be uniform unless the final correct shape of the Taylor bubble is obtained.
7. The bubble surface is displaced locally according to the departure of the surface pressure from uniformity.
8. The bubble surface adjusted thus may not be normal to the axis of symmetry at the nose (stagnation point) because this is dependent on the chosen bubble velocity U_{TB}. The value of U_{TB} is therefore adjusted so as to lead to the required tangency condition.
9. The above steps are repeated until convergence to the final solution (which includes the bubble shape and its velocity) is attained.

4. INTERFACE AND MESH ADJUSTMENTS

The liquid flow field is primarily influenced by the shape of the Taylor bubble and this is not known in advance. In order to determine the bubble shape, a certain physical condition has to be satisfied; the pressure drop over the Taylor bubble must be zero, as has been found by experiment. Thus, the pressure on the gas side of the surface must be uniform and is taken as the pressure at the stagnation point at the nose of the Taylor bubble. The pressure along the bubble interface resulting from the calculation of the flow field combined with surface tension stress must therefore match this uniform pressure, and if it does not, the surface must be moved. An iterative method is developed below which utilises the above principle to find the appropriate displacement of the surface according to the departure of the gas pressure from uniformity.

The non-orthogonal mesh is fitted to the bubble surface by placing the vertices of each cell on this surface (see Fig. 3). The concept used here to shift these vertices is based on the fact that a change in cell face area (e.g. A_e) caused by the movement of the cell face s will correspond to a change in the velocity at the cell face, v_e (which is the component aligned along the surface), so as to keep the flow rate through face e the same. This change in velocity will correspond to a change in pressure gradient $(p_E - p_P)$, which is directly related to the amount by which the surface pressures at faces are required to change. This concept therefore relates the desired surface pressure adjustment directly to the displacement of the cell vertices.

Let the required uniform pressure along the bubble surface be p_0; let δp_s and δp_{se} be the difference between the intermediately computed surface pressures and p_0. Now, since the surface pressures are obtained from extrapolation of the liquid pressure field, it follows that:

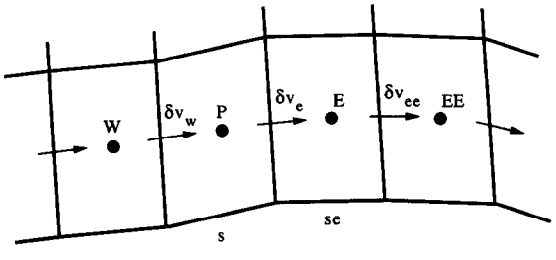

Fig. 3. Mesh cells along the Taylor bubble surface.

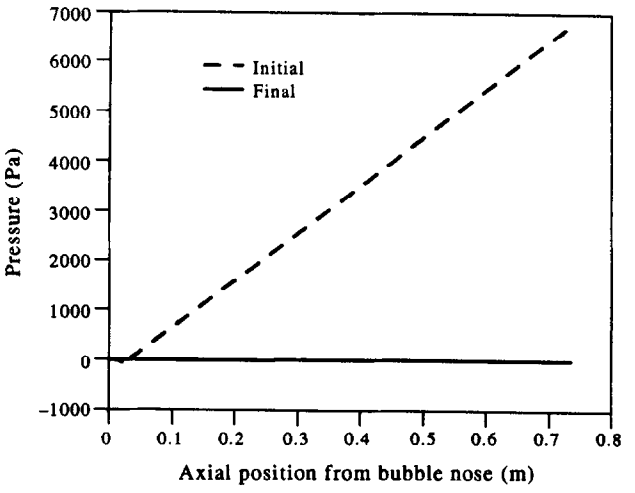

Fig. 4. Initial and final bubble surface pressure.

$$\delta p_p \doteq \delta p_s \tag{23}$$

and

$$\delta p_E \doteq \delta p_{se} . \tag{24}$$

These pressure changes would result in adjustments in cell face velocities v_e, v_{se}, etc. The relationship between these adjustments is derived from an approximate one-dimensional finite difference momentum equation which relates the velocity adjustments to the pressure increments, thus

$$a_p \delta v_e = a_w \delta v_w + a_e v_{ee} - d_e(\delta p_E - \delta p_p) . \tag{25}$$

In the above equations, the a and d coefficients are obtained from corresponding values pertaining to the main finite difference equations solved for the nodal values of the velocity components u_i. Equation (25) represents a tridiagonal matrix set of equations which can be solved for all δvs given δp_P, δp_E, etc.

Now the mass flux through each cell face, such as e, is given by

$$F_e \propto v_e A_e . \tag{26}$$

The assumption is now introduced that a change in v_e does not result in any change in F_e. Hence

$$\delta F_e = 0$$

and

$$A_e \delta v_e + v_e \delta A_e = 0$$

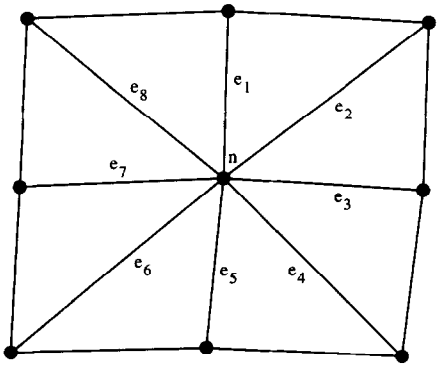

Fig. 5. Structure and interconnections used for remeshing.

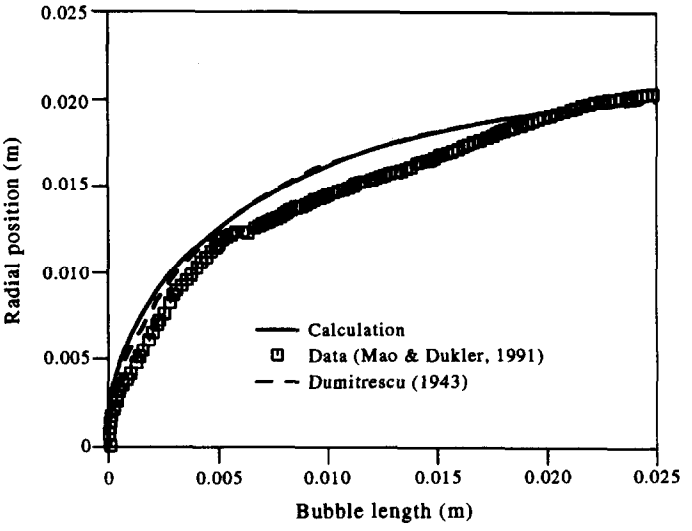

Fig. 6. Bubble nose shape.

i.e.

$$\delta A_e = -\frac{A_2}{v_e}\delta v_e . \tag{27}$$

Equation (27) can now be used directly to determine δA_e given δv_e which was found from the solution of equation (25).

The surface of the bubble may now be displaced according to the δA values that have just been found. This procedure is applied at the end of either every outer iteration or several iterations until convergence, which is deemed to be reached when the surface pressure is within 0.05% of the uniform value required.

It was found that in the initial stages of the computation, the displacements in the proximity of the nose were, in some cases, of the order of 15% of the tube diameter. These large displacements propagated along the surface as the solution evolved and in some cases led to an unstable process. A number of remedies were found to cope with this behaviour, the best of which was one where the displacements were under-relaxed such that the maximum change in a cell face area was limited to 10%. This is explained by the fact that the surface pressure is highly sensitive to a displacement of the surface. Also, the solution for the flow field was permitted to develop over an initial number of iterations, say 30, before the surface was displaced at every iteration. An example of the surface pressure distributions along the bubble at the beginning and the end of a calculation when uniform pressure is achieved are displayed in Fig. 4.

After displacement of the bubble surface, a new mesh has to be found. Rather than generating a completely new mesh which is a tedious task, the original mesh is rearranged according to the automated procedure described below.

The remeshing process is based on the theory of large elastic deformations of structures. The mesh is considered as a pin-jointed frame which in its equilibrium state will satisfy

$$\sum_{ic=1}^{N} f_j^{ic}(n) = 0 \tag{28}$$

at each node n where N is the number of interconnections to node n, $j = 1,2,3$ and f is the force acting on each interconnection. The number and structure of the interconnections employed, in order to maintain a good resemblance to the initial mesh as it is remeshed, may be seen in Fig. 5. If the mesh is to be displaced, a force given by

$$f^{ic}(n) = \frac{E}{L_{ic}}\delta_{ic}\cos\alpha \tag{29}$$

must act on each interconnection ic, where E is the elastic modulus, L_{ic} is the initial length of interconnection ic, $\cos\alpha$ is the directional cosine and δ_{ic} is the change in length of interconnection ic. The 'elastic' modulus E may be varied throughout the mesh depending on whether it is deemed necessary to remesh sections of the mesh or rigidly retain its shape. An iterative procedure is formulated where the displacement at each node is computed using equation (29); the coordinates are then updated and the procedure is repeated until equation (28) is satisfied for all nodes. The extra storage requirement to remesh the domain is minimal, requiring only two additional arrays to store the coordinates of the original mesh. The computing effort to iteratively remesh the domain is only a small fraction of that required to generate a new mesh. The method was found to be flexible and the mesh can be prevented from folding over on itself by under-relaxing the intermediate displacements.

5. RESULTS

The proposed model is now applied to calculate the shape, rise velocity and pressure drop for: (i) the case of a single Taylor bubble rising in stagnant liquid; (ii) the case of a single Taylor bubble rising in flowing liquid; and (iii) the case of a train of Taylor bubbles as happens in slug flow. For all cases, an initial guess of the Taylor bubble shape must be made and a non-orthogonal mesh must be generated to accommodate this initial shape. For the present study the initial shape is taken as a cylindrical body with a spherical nose. The flow domain is split into separate subdomains in

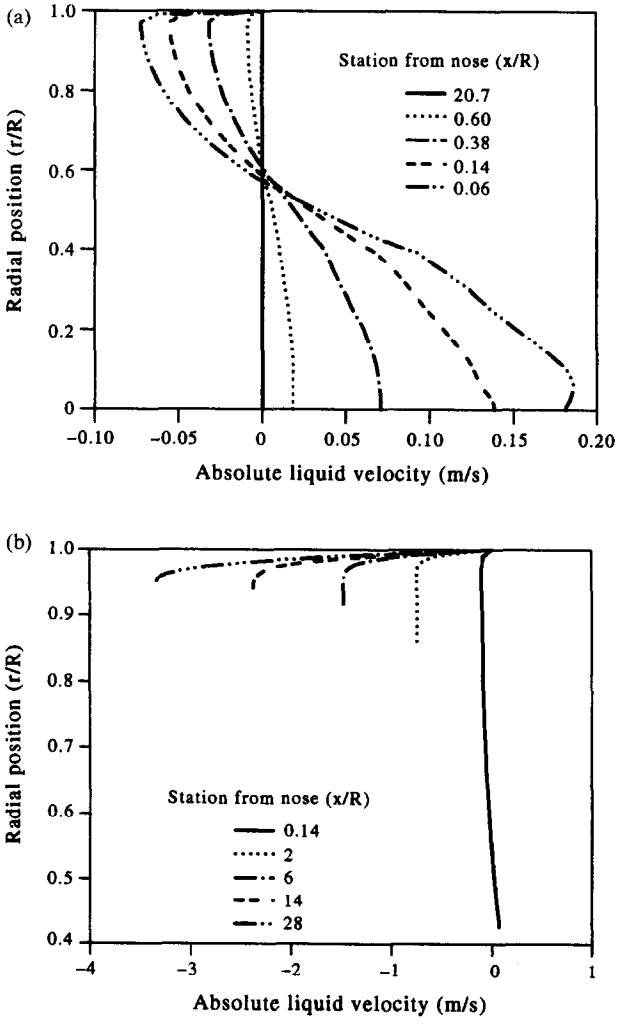

Fig. 7. Profiles of the absolute velocity (a) ahead of the bubble nose and (b) in the liquid film.

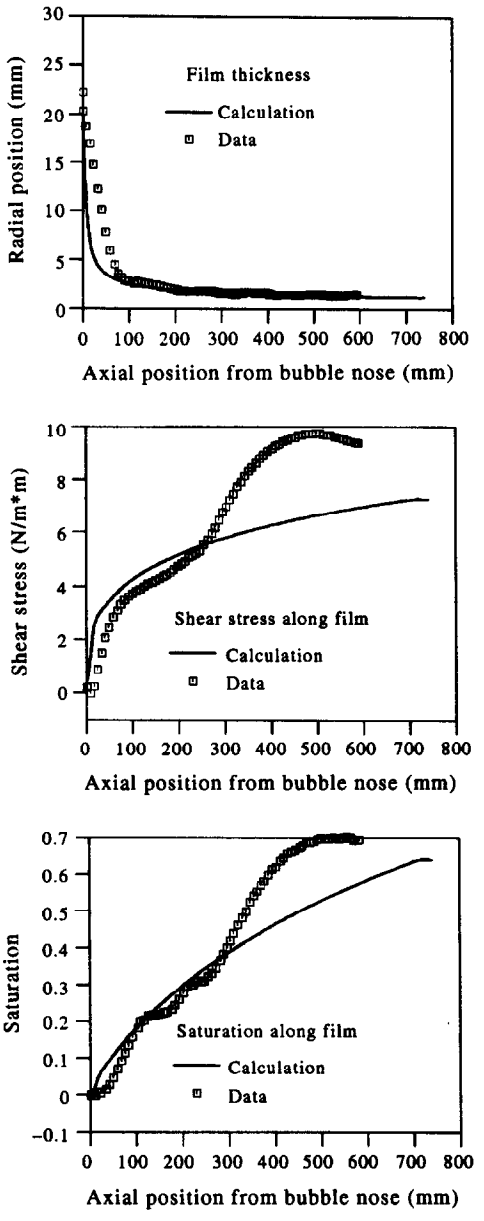

Fig. 8. Profiles of the film thickness, shear stress and saturation for a single Taylor bubble compared against measured profiles of Mao and Dukler [28].

order to create a suitable mesh by the block-structured mesh generator; 11 blocks in total were used. The most important area of interest is the local flow around the Taylor bubble surface and so mesh cells were concentrated close to this surface. For example, in case (i) a block consisting of 30 mesh cells in the radial direction and 70 in the axial direction was used in the vicinity of the nose (see Fig. 2). For the liquid film, 30 mesh cells were used in the radial direction and between 150 and 250 in the axial direction depending on the length of the Taylor bubble. In the recirculation zone behind the base, four blocks were constructed to give a 60 × 600 cell mesh; this mesh was non-uniformly distributed so as to concentrate cells close to the base. At the front of the Taylor bubble two further blocks were generated to give an overall mesh of 50,000 cells in total. Two similar mesh configurations were employed for cases (ii) and (iii), one with a total of 8960 cells, the other with 51,150 cells. The fine mesh was used to verify the grid independence of the results. The initial guessed Taylor bubble shape in each case occupied 80% of the tube diameter and calculations were made for air bubbles rising in water, for which surface tension was ignored. Two pipe diameters were used, these were 0.05 m for all cases and additionally 0.0276 m for cases (ii)

and (iii). The pipe length for case (i) was 6 m, and the range of length ratios (L_{TB}/L) for cases (ii) and (iii) were 0.15–0.46 and 0.42–0.55, respectively. The number of iterations required to converge was approximately 1000 iterations for case (i), for example. Of course this number depends on the chosen initial shape of the Taylor bubble and can be greatly reduced with a more accurate guess.

(i) Single Taylor bubble rising in stagnant liquid: the computed shape of the Taylor bubble is compared with both that measured by Mao and Duckler [20] and the analytical profile obtained by Dumitrescu [9] in Fig. 6. The agreement with the data in the proximity of the stagnation point, where zero tangency is expected, is very good, although there is a discrepancy over the remainder of the nose. This may be attributed to strong miniscus effects, reflected in the wavy nature of the interface, which were experienced by Mao and Duckler during their experiments and where it was only possible to measure very few distinct bubbles. However, agreement with the Dumitrescu profile is seen to be excellent over the entire nose. The surface computed here can be seen to be smooth and this was achieved without the need for any special smoothing technique such as that to which Mao and Duckler [21] resorted; the pressure over the surface can also be seen to be uniform in Fig. 4.

The computed velocity profiles at different axial stations ahead of the bubble nose and in the liquid film are shown in Fig. 7. The influence exerted by the rising Taylor bubble on the stagnant liquid ahead of it is to push the liquid aside into the falling film. This may be seen in Fig. 7, where the velocity ahead of the bubble is no longer uniform but accelerates to a value almost equal to the bubble velocity, turns negative close to the wall and remains negative in the falling film. The negative velocities ahead of the bubble nose persist for up to 20 tube diameters upstream of the bubble nose and it is clear that the position at which reverse flow occurs extends well beyond the beginning of the falling film.

In Fig. 8, profiles of the calculated film thickness, wall shear stress and saturation (defined as $\phi = \tau_w/\rho g h$, where h is the film thickness) are compared against the measured profiles of Mao and Duckler [20]. The agreement with the data beyond the first 100 mm of the film thickness is good except for a small discrepancy. The shear stress over the first 300 mm of the film is close to the data but departs thereafter. This is thought to be associated with the point at which the film goes through the transition between laminar and turbulent flow, which is also evident in the wavy nature of the interfaces. The computation, however, was carried out on the assumption that the flow remains laminar throughout the film. A proper account of the transition to turbulent flow is needed to enable a meaningful comparison with the data in that region and is beyond the scope of this work. The saturation, which expresses the degree of balance between the wall shear stress and the gravitational force, should asymptotically approach unity along the film. It can be seen from Fig. 8 that agreement with the data is good up to the point of transition.

The unique shape of the Taylor bubble is determined by a unique rise velocity which produces a nose shape which is locally spherical. The value of the rise velocity found to match this condition was 0.246 m s^{-1}. This corresponds to a Froude number of 0.351, where the Froude number is

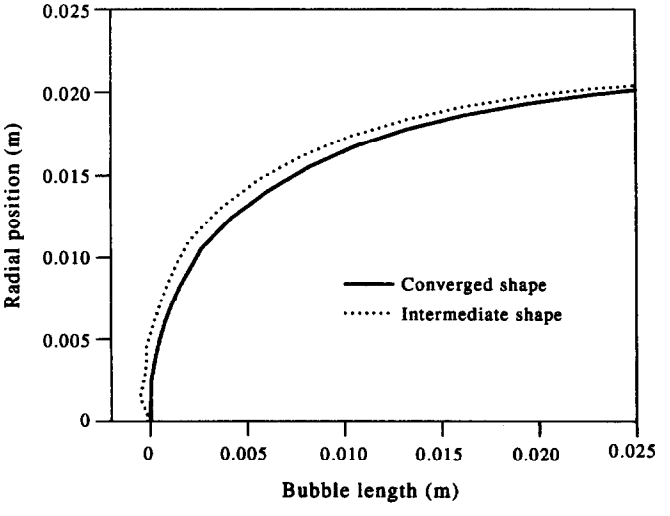

Fig. 9. Final and intermediate computed bubble profile.

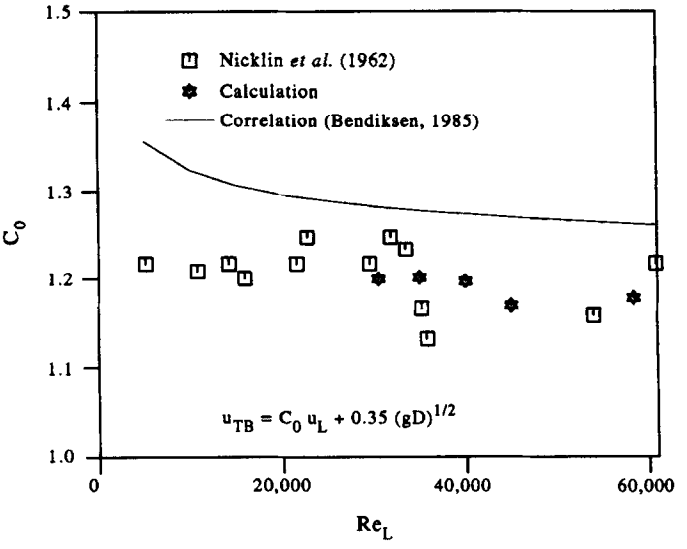

Fig. 10. Rise velocity of single Taylor bubble in flowing liquid.

defined by $Fr = U_{TB}/\sqrt{(gd)}$. This result shows good agreement with the experimental values of 0.35, 0.353 and 0.36 of Dumitrescu [9], Mao and Duckler [20] and Maneri [28], respectively, the analytic value of 0.36 obtained by Vanden-Broeck [29] and Couet *et al.* [30] and the computational value of 0.345 of Mao and Duckler [21]. The correct nose shape of the Taylor bubble which corresponds

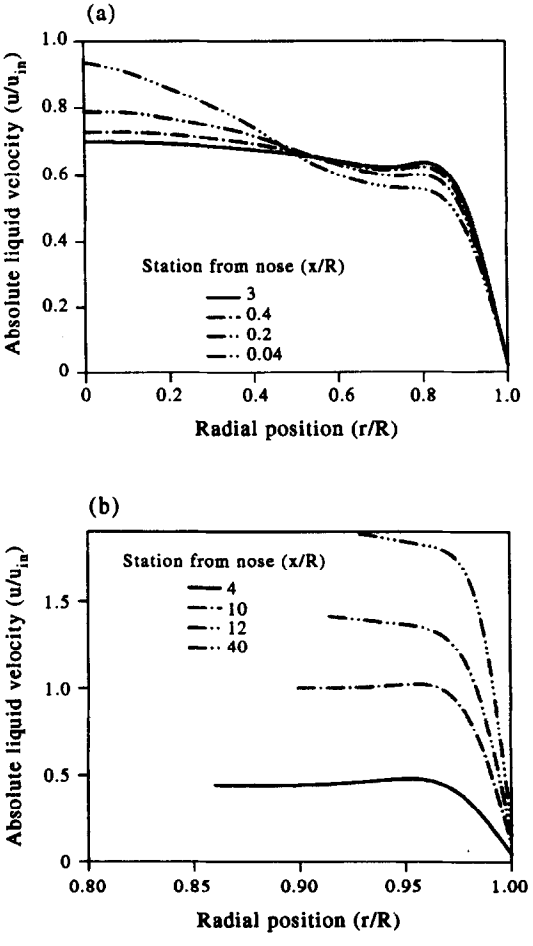

Fig. 11. Profiles of absolute velocity (a) ahead of the bubble nose and (b) in the liquid film.

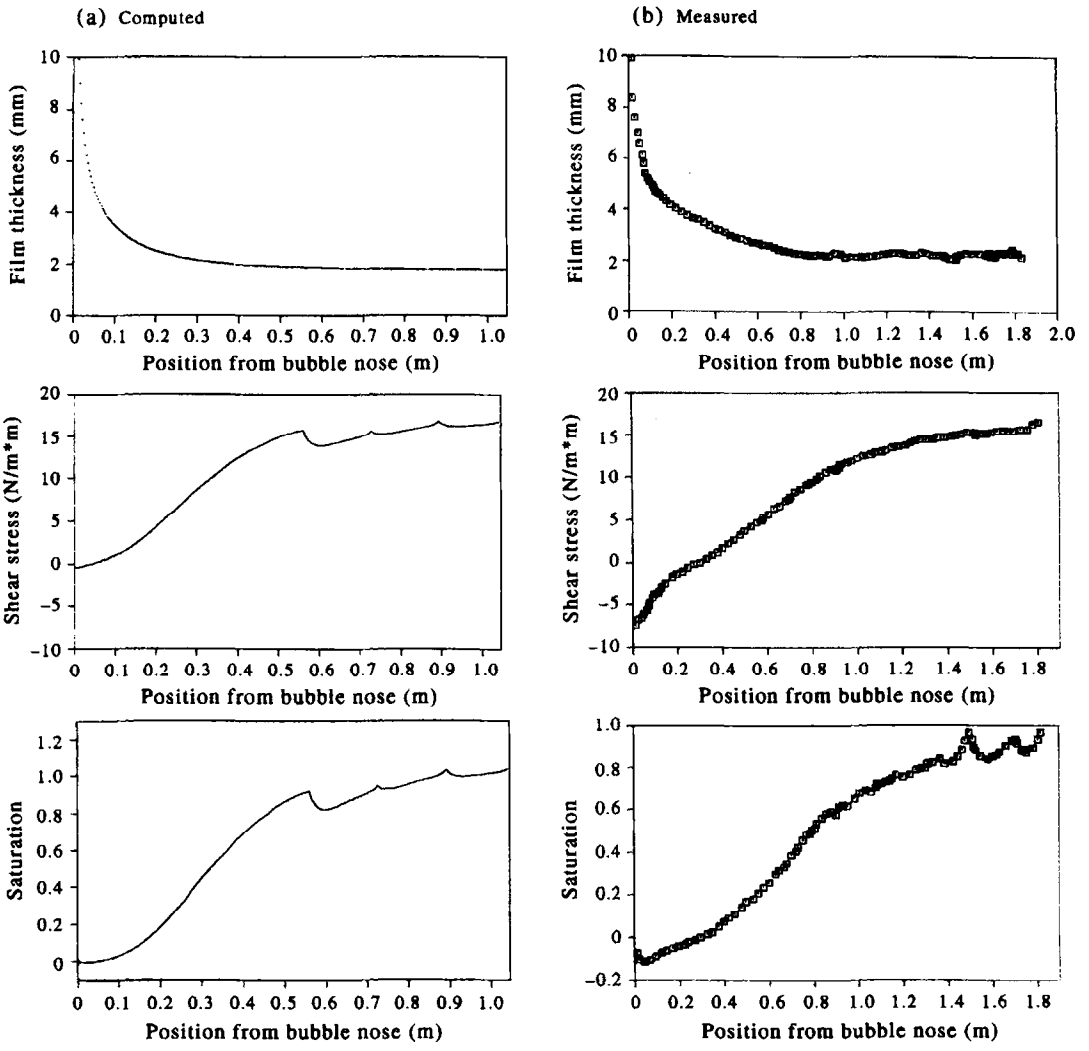

Fig. 12. Profiles of film thickness, shear stress and saturation compared with typical profiles measured by Mao and Dukler [19] for 0.322 m s^{-1}.

to this rise velocity is compared in Fig. 9 with one obtained in the intermediate stages of the computations.

(ii) Single bubble rising in flowing liquid: the radial profiles for the velocity, k and ϵ inlet were taken as those of turbulent fully developed pipe flow. Simulations were carried out for a range of mean liquid velocities ranging from 0.61 to 1.182 m s^{-1} and Taylor bubble lengths ranging from 0.25 to 1.15 m covered by the experiments of Nicklin *et al.* [12]. Figure 10 shows the results of these simulations where the value of C_{02} in equation (3) is plotted against the mean liquid Reynolds number. The excellent agreement between the calculated bubble rise velocity and that measured by Nicklin *et al.* [12] suggests that the model closely approximates reality. The computed profiles of velocity at different axial stations ahead of the bubble nose and in the liquid film are shown in Fig. 11. In Fig. 12, (a) profiles of the calculated film thickness, wall shear stress and saturation are compared against typical measured profiles (b), taken from Mao and Duckler [19]. It should be emphasized here that the flow calculations do not correspond to the same flow conditions of the experiments since the latter were not obtainable from the reference. Comparison between calculation and experiment must therefore be confined to trends. Reverse flow in the liquid film occurs at about 0.9 tube diameters from the bubble nose. This may be seen in Fig. 11 where the profiles in this proximity turn negative. The wall shear stress correspondingly changes sign at this location (Fig. 12). Also, the trend of increasing shear stress along a similar slope, then forming a plateau is consistent with the measured one. The plateau is located 10 tube diameters from the bubble nose at which the bubble is sufficiently long to maintain a film of almost constant thickness.

The gradients of both the velocity and turbulence kinetic energy progressively diminish to zero beyond this location. The saturation profile lends further evidence to the belief that the film has reached an equilibrium thickness by the fact that it tends to asymptote to unity.

(iii) Periodic slug flow: the range of conditions considered are the same as those in the preceding case. The ratio of the length of the Taylor bubble to that of the liquid slug for the 0.0276 and 0.05 m diameter tubes ranged from 0.15 to 0.46 and from 0.42 to 0.55, respectively. These values correspond to those experimentally observed by Akagawa *et al.* [31] and Fernandes [18], for air–water slug flow with U_{SL} ranging from 1.0 to 1.5 m s^{-1} and from 0.49 to 0.8 m s^{-1}, respectively, and U_{SG} ranging from 0.8 to 1.2 m s^{-1} and from 0.4 to 1.2 m s^{-1}, respectively, giving a superficial mixture Reynolds number in excess of 30,000. To simulate the periodic passage of Taylor bubbles and liquid slugs, the cyclic boundary conditions mentioned earlier are now imposed.

First, the computations were carried out assuming that the liquid is free of gas. The results showed that the profiles for velocity and other variables in the liquid slug are quite different from those obtained in the single bubble case. Figure 13 contrasts the profiles for velocity and turbulence quantities obtained from the cyclic conditions with the fully developed pipe profiles that are used for the single bubble case. The difference in profiles, however, did not appear to influence the predicted rise velocity: the computed value differed little from the single bubble case. This is at variance with the data which suggest that the rise velocity in continuous slug flow should be considerably higher. Figure 14 plots the computed value of C_{02} against the measurements of Fernandes [18]; it shows that the data are underpredicted by more than 30%.

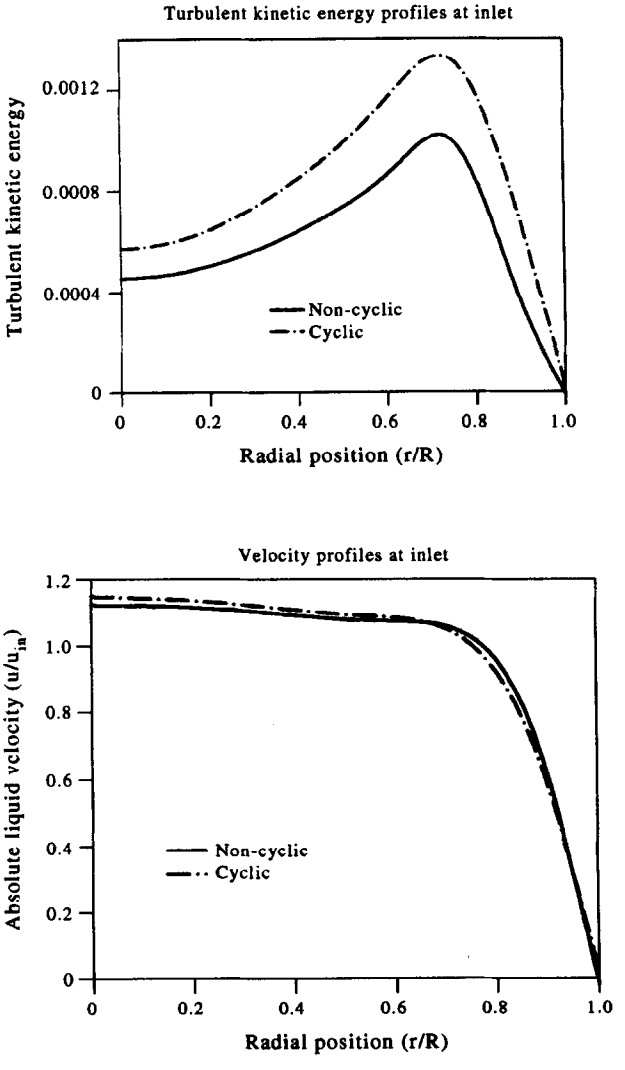

Fig. 13. Profiles for cyclic and non-repeating slug flow.

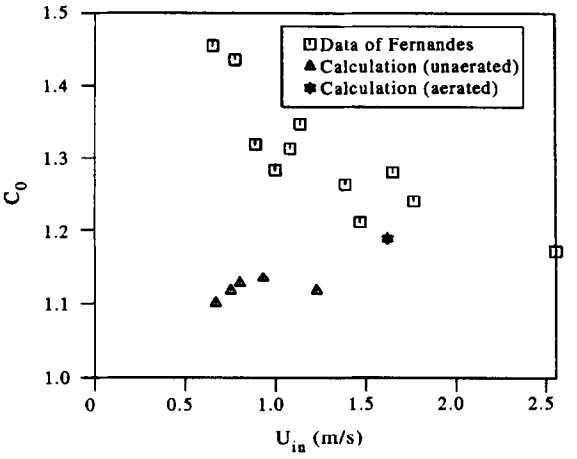

Fig. 14. Rise velocity in unaerated slug flow.

The above discrepancy is attributed to the assumption that the liquid slug was free of gas which in the case of periodic slug flow is not true. This was then remedied by considering that the slug fluid was a mixture of both liquid and dispersed gas which are homogeneously dispersed into each other, and that they flow at the same velocity. The gas fraction present in this form was taken to range from 20 to 30%, which corresponds to the experimental average values of Akagawa *et al.* [31]. No mass transfer between the gas in the slug and the Taylor bubble was assumed to take place.

With the above assumptions, the computed value of the bubble velocity was then found to be much closer to the measured value as can be seen in Fig. 15. The scatter of the computed values is related to the various cases with different pipe diameters but the variance is seen to be within 10% of the C_{02} value of 1.2. This seems quite reasonable in view of the large scatter of experimental values and considering the crude way in which the presence of the gas bubbles in the liquid slug is accounted for. It nonetheless does point out that to obtain accurate predictions of slug flow features, account must be taken of the small gas bubbles dispersed in the liquid slug and that future work should focus on the modeling of this phenomenon.

In Fig. 16, the pressure gradient is plotted as a function of U_{SG} for U_{SL} equal to 1 and 1.5 m s^{-1}, the experimental data shown are those of Akagawa *et al.* [31]. The computed results are seen to be in fair agreement with those calculated. The discrepancy may again be attributed to the crude method used to account for the dispersed phase in the liquid slug. However, the agreement is very encouraging and further work is needed to more accurately model the effects of the liquid slug void fraction by, for example, the two fluid model.

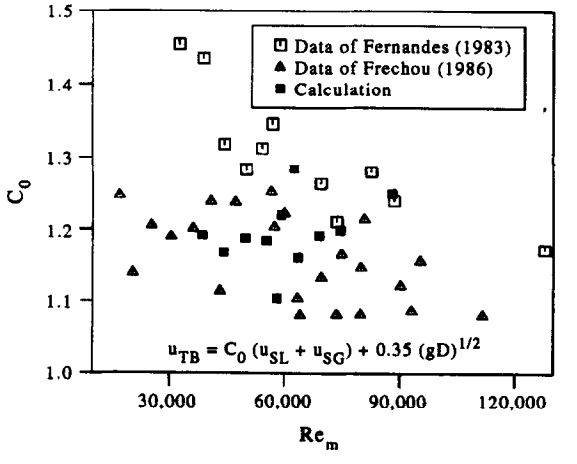

Fig. 15. Rise velocity in slug flow.

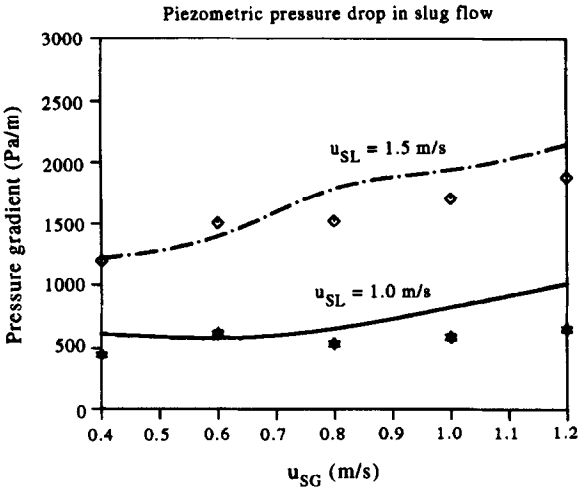

Fig. 16. Comparison of pressure gradient for 1.5 and 1.0 m s^{-1} with the data of Akagawa *et al.* [31].

Finally, the relative and absolute velocity vector fields of the flow around the Taylor bubble nose and behind its base are shown in Figs 17 and 18, respectively. It may be seen that the liquid is swept into the film and flows downward into the recirculation zone behind the base.

6. CONCLUSIONS

The liquid flow field, both laminar and highly turbulent, around Taylor bubbles rising in vertical tubes is analyzed using a finite volume computational procedure that solves the transport equations

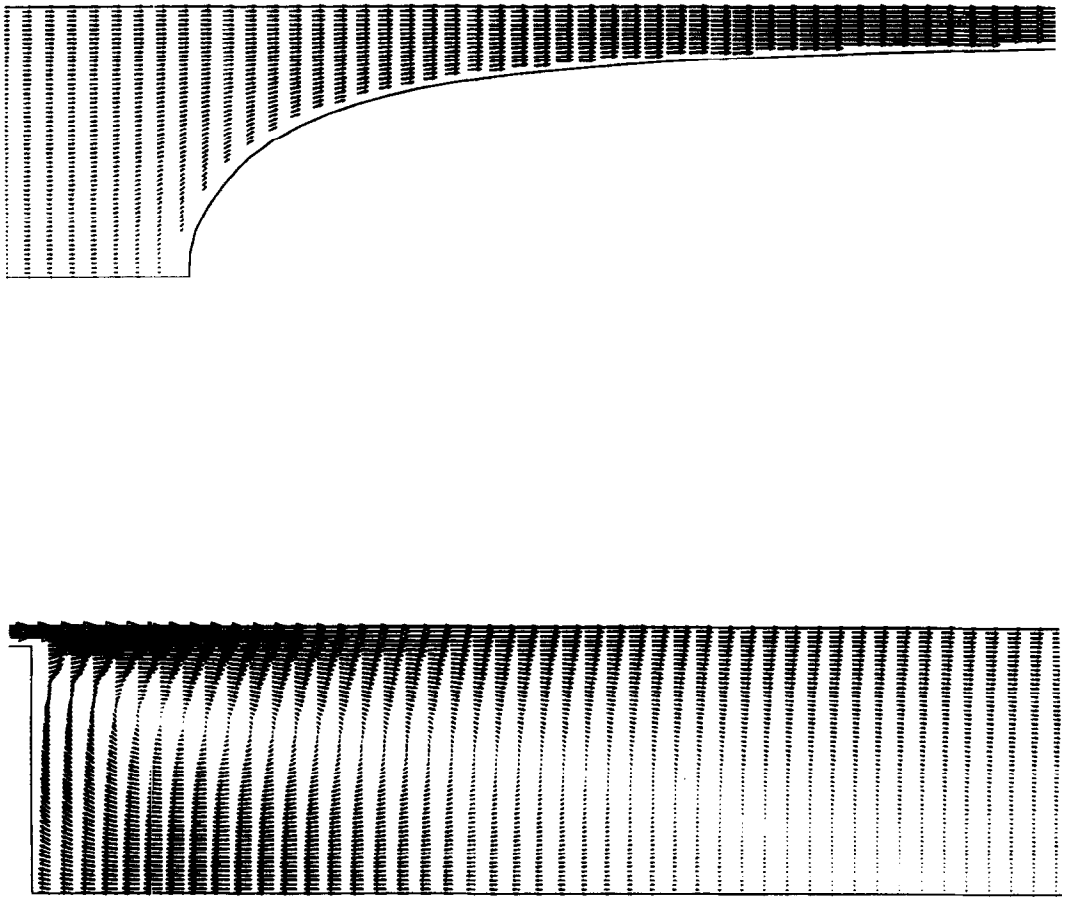

Fig. 17. Relative velocity field around bubble nose and behind its base.

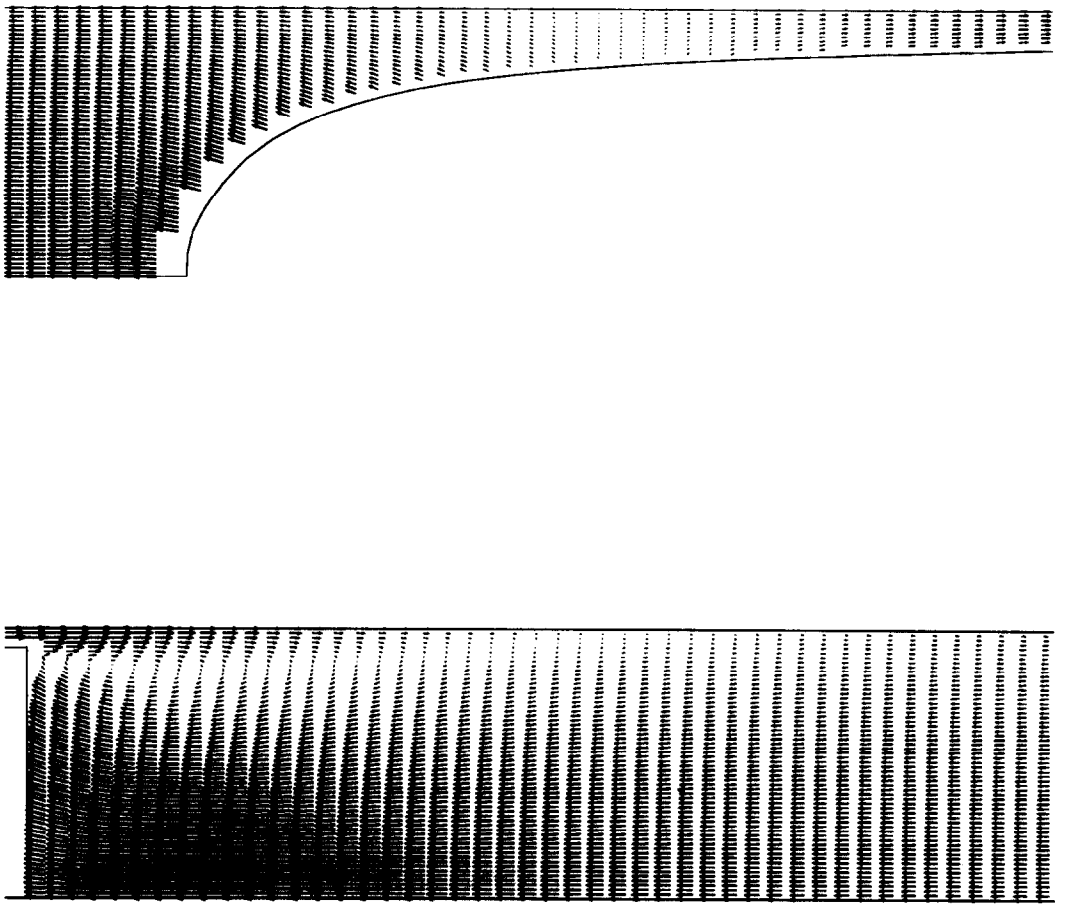

Fig. 18. Absolute velocity field around bubble nose and behind its base.

on a non-orthogonal block-structured mesh. The method determines the shape of the bubble and its rise velocity from the conditions of constant pressure within the bubble and smoothness of the bubble nose at the axis. The method also incorporates cyclic boundary conditions at inlet and outlet for periodic slug flow and a very simple but empirical means of accounting for the presence of dispersed gas in the liquid slug for this case is introduced.

Calculations using the method for laminar water flow around a single air bubble are compared with inviscid flow analysis and experiment. It is found that the computed shape of the bubble and its rise velocity are in good agreement with both data and other solutions.

The method was further applied to the case of gas-free liquid flowing around a single Taylor bubble and to periodic slug flow, and the calculations were compared with experiment. It was found that the rise velocity accords extremely well with experiment in the first case, while in the second reasonable agreement is obtained only when the presence of dispersed gas in the slug is accounted for, though this was done approximately.

It may be concluded that a model is necessary to account for the dispersed gas phase within the slug if the empiricism introduced by the present treatment is to be avoided. The model should also account for gas mass transfer between the liquid slug and the Taylor bubble through entrainment and shedding mechanisms.

Acknowledgement—This work was supported by the SERC/MTD.

REFERENCES

1. Fancher, G. H. and Brown, K. E., Prediction of pressure gradients for multiphase flow in tubing. *Soc. Pet. Engng J.*, March 1966, 59–69.
2. Hughmark, G. A., Holdup and pressure drop with gas-liquid flow in a vertical pipe. *Chem. Engng Proc.*, 1961, **58**, 62.
3. Yocum, B. T., Paper 924-G, SPE 32nd Annual Fall Meeting, Dallas, TX, October 1959.

4. Duns, H. and Ross, N. C. J., Vertical flow of gas and liquid mixtures in wells. *Proc. Sixth World Petroleum Congress*, Frankfurt, 19–26 June 1963, Section II, Paper 22-PD6, pp. 451-465.
5. Griffith, P. and Wallis, G. B., Two-phase slug flow. *J. Heat Transfer*, 1961, **83,** 307–320.
6. Fernandes, R. C., Semiat, R. and Dukler, A. E., A hydrodynamic model for gas-liquid slug flow in tubes. *AIChE J.*, 1983, **29,** 981–989.
7. Orell, A. and Rembrand, R., A model for gas-liquid slug flow in vertical tubes. *AIChE J.*, 1986, **29,** 981–989.
8. Issa, R. I. and Tang, Z., Modelling of vertical gas-liquid slug flow in pipes. ASME Annual Winter Meeting, Dallas, TX, 25–30 November 1990.
9. Dumitrescu, D. T., Stromung i an einer luftblase in senkrechten rohr. *Z. Angew. Math. Mech.*, 1943, **23,** 139–149.
10. Davies, R. M. and Taylor, G. I., The mechanism of large bubbles rising through extended liquids and through liquids in tubes. *Proc. R. Soc. London, Ser. A*, 1950, **200,** 375–390.
11. Harmathy, T. Z., Velocity of large drops and bubbles in media of infinite or restricted extent. *AIChE J.*, 1960, **6,** 281–288.
12. Nicklin, D. J., Wilkes, J. O. and Davidson, J. F., Two phase flow in vertical tubes. *Trans. Inst. Chem. Engrs*, 1962, **40,** 61–88.
13. Collins, R., A simple model of the plane gas bubble in a finite liquid. *J. Fluid Mech.*, 1965, **22,** 763.
14. Collins, R., de Moraes, F. F., Davidson, J. F. and Harrison, D., The motion of large bubbles rising through liquid flowing in a tube. *J. Fluid Mech.*, 1978, **89,** 497.
15. Nickens, H. V. and Yannitell, D. W., The effects of surface tension and viscosity in the rise velocity of a large gas bubble in a closed vertical liquid-filled tube. *Int. J. Multiphase Flow*, 1987, **13,** 57–69.
16. Bendiksen, K. H., On the motion of long bubbles in vertical tubes. *Int. J. Multiphase Flow*, 1985, **11,** 797–812.
17. Frechou, D., Etude de l'écoulement ascendant à trois fluides en conduite verticale. These Inst. Natl. Polytech., Toulouse, France, 1986.
18. Fernandes, R. C., Experimental and theoretical studies of isothermal upward gas-liquid flows in vertical tubes. Ph. D. thesis, University of Houston, TX, 1981.
19. Mao, Z. S. and Duckler, A. E., An experimental study of gas-liquid slug flow. *Expts Fluids*, 1989, **8,** 169–182.
20. Mao, Z. S. and Duckler, A. E., The motion of Taylor bubbles in vertical tubes II. Experimental data and simulations for laminar and turbulent flow. *Chem. Engng Sci.*, 1991, **46**(8), 2055–2064.
21. Mao, Z. S. and Duckler, A. E., The motion of Taylor bubbles in vertical tubes I. A numerical simulation for the shape and rise velocity of Taylor bubbles in stagnant and flowing liquid. *J. Comp. Phys.*, 1990, **91,** 132–160.
22. Nagano, Y. and Hishida, M., Improved form of the k-ϵ model for wall turbulent shear flow. *J. Fluid Engng*, 1987, **109,** 156–171.
23. Launder, B. E. and Spalding, D. B., The numerical computation of turbulent flows. *Comp. Meth. Appl. Mech. Engng*, 1974, **3,** 269.
24. Rhie, C. M. and Chow, W. L., Numerical simulation of the turbulent flow past an aerofoil with trailing edge separation. *AIAA J.*, 1983, **21**(11), 1525.
25. Peric, M., Ph. D. thesis, Imperial College, University of London, 1985.
26. Zienkiewicz, O. C. and Irons, B. M., Isoparametric elements. In *Finite Element Techniques*, ed. H. Tottenham and C. Bressca, Seminar at University of Southampton, April 1970.
27. Patankar, S. V. and Spalding, D. B., A calculation procedure for heat, mass and momentum transfer in three-dimensional parabolic flows. *J. Heat Mass Trans.*, 1972, **15,** 1787.
28. Maneri, C. C., Ph.D. dissertation, Polytechnic Institute of Brooklyn, NY, 1970.
29. Vanden-Broeck, J.-M., Rising bubbles in a 2-dimensional tube with surface tension. *Phys. Fluids*, 1984, **27,** 2604.
30. Couet, B., Strumolo, G. S. and Ziehl, W., Effects of surface tension and tube inclination on a two-dimensional rising bubble. *Third Int. Conf. on Multiphase Flow*, The Hague, The Netherlands, 18–20 May 1987.
31. Akagawa, K., Hamaguchi, H., Sakaguchi, T. and Ikari, T., Studies on the fluctuation of pressure drop in two-phase slug flow. *Bulletin of JSME*, 1971, **14,** 447–454.